Author Manuscript

Author Manuscript

Author Manuscript

Author Manuscript

HHS Public Access

Author manuscript

Proc SPIE Int Soc Opt Eng. Author manuscript; available in PMC 2017 July 21.

Published in final edited form as:

Proc SPIE Int Soc Opt Eng. 2017 February 11; 10133: . doi:10.1117/12.2254613.

Structural-Functional Relationships Between Eye Orbital Imaging Biomarkers and Clinical Visual Assessments

Xiuya Yao[a], **Shikha Chaganti**[b], **Kunal P. Nabar**[b], **Katrina Nelson**[c], **Andrew Plassard**[b], **Rob L. Harrigan**[c], **Louise A. Mawn**[d], and **Bennett A. Landman**[b,c]

[a]Department of Biomedical Informatics, Vanderbilt University, 2525 West End Ave #1475, Nashville, TN 37203

[b]Computer Science, Vanderbilt University, 2301 Vanderbilt Place, Nashville, TN USA 37235

[c]Electrical Engineering, Vanderbilt University, 2301 Vanderbilt Place, Nashville, TN USA 37235

[d]Vanderbilt Eye Institute, Vanderbilt University School of Medicine, 2311 Pierce Avenue, Nashville, TN USA 37232

Abstract

Eye diseases and visual impairment affect millions of Americans and induce billions of dollars in annual economic burdens. Expounding upon existing knowledge of eye diseases could lead to improved treatment and disease prevention. This research investigated the relationship between structural metrics of the eye orbit and visual function measurements in a cohort of 470 patients from a retrospective study of ophthalmology records for patients (with thyroid eye disease, orbital inflammation, optic nerve edema, glaucoma, intrinsic optic nerve disease), clinical imaging, and visual function assessments. Orbital magnetic resonance imaging (MRI) and computed tomography (CT) images were retrieved and labeled in 3D using multi-atlas label fusion. Based on the 3D structures, both traditional radiology measures (e.g., Barrett index, volumetric crowding index, optic nerve length) and novel volumetric metrics were computed. Using stepwise regression, the associations between structural metrics and visual field scores (visual acuity, functional acuity, visual field, functional field, and functional vision) were assessed. Across all models, the explained variance was reasonable ($R2 \sim 0.1–0.2$) but highly significant ($p < 0.001$). Instead of analyzing a specific pathology, this study aimed to analyze data across a variety of pathologies. This approach yielded a general model for the connection between orbital structural imaging biomarkers and visual function.

Keywords

visual function; eye; MRI; CT; multi-atlas; orbital structure

1. INTRODUCTION

The onset of eye diseases and impairment of vision are often accompanied by changes in physical characteristics of eye orbital structures. These changes in orbital structures may play a significant role in the progression or recurrence of eye diseases. Magnetic resonance imaging (MRI) of the eye orbit can be used to assess the risk and progression of optic

Author Manuscript Author Manuscript Author Manuscript Author Manuscript

diseases and visual loss [22]. Imaging data after damage to the orbit of the eye in trauma situations can be related to decline in visual function [21]. Orbital metrics of the eye such as Barrett Index have also been shown to be associated with dysthyroid optic neuropathy in patients with Graves' orbitopathy [19–20].

Other studies show on a case-by-case basis that orbital structure does not just have an effect on eye function, but can also be used as a predictive measure for the decline of visual function [19–21]. The orbit is a complex environment— many different factors affect orbital structure and loss of vision. However, these studies suggest that a deeper relationship exists between orbital structure and the onset of optic conditions. The goal of this study was to explore the relationship between clinical and structural metrics by correlating large sets of structural metrics (e.g., Barrett Index) with the clinically obtained visual field scores (e.g., visual acuity score). This was done in order to determine if a relationship between the two could be obtained, or if a general statistical model for the relationship between the orbital structure metrics of the eye and visual field scores can be determined.

The subjects in this study were selected because they had either computed tomography (CT) or magnetic resonance imaging (MRI) performed on the orbit of the eye as a regular part of their clinical care. They all had clinical visual disability scores available as well. An experienced undergraduate manually labeled approximately 20 subjects of each MRI and CT imaging modality. Then, multi-atlas segmentation was performed to segment the extraocular rectus muscles, eye globes, optic nerves, and orbital fat [2,3]. Twenty-one different structural metrics were then calculated from the segmentation pipelines. For each visual metric, a stepwise regression function fit a generalized linear model to a Poisson distribution in order to determine the amount of variance in visual function metrics that can be explained by the structural metrics of the eye orbit.

2. METHODS

2.1 Patient Data

The relationship between visual function and MRI/CT-derived orbital structures were investigated in a retrospective cohort of patients at Vanderbilt University Medical Center. Subjects were selected based on both having met clinical criteria for eye disease and undergoing CT or MRI imaging as part of their regular clinical care. The eye diseases incorporated in this study are: *Thyroid Eye Disease*: toxic diffuse goiter without thyrotoxic crisis or storm (242.00), endocrine exophthalmos (376.2*), thyrotoxic exophthalmos (376.21), exophthalmic opthalmoplegia (376.22); *Orbital Inflammation*: acute inflammation of the orbit (376.0), acute inflammation of the orbit unspecified (376.00), orbital cellulitis (376.01), orbital periotisis (376.02), chronic inflammation of orbit unspecified (376.10), orbital granuloma (376.11), orbital myositis (376.12); *Optic Nerve Edema*: benign intracranial hypertension (348.2); *Glaucoma*: low-tension open angle glaucoma (365.12); *Intrinsic Optic Nerve Disease*: optic neuritis (377.3), optic neuritis unspecified (377.30), optic pappilitis (377.31), retrobular neuritis (acute), nutritional optic neuropath (377.33), toxic optic neuropathy (377.34), other optic neuritis (377.39), other disorders of the optic nerve (377.4), ischemic optic neuropathy (377.41), hemorrhage in optic nerve sheaths (377.42), optic nerve hypoplasia (377.43), other disorders of the optic nerve (377.49).

Author Manuscript Author Manuscript Author Manuscript Author Manuscript

The study was conducted on 470 subjects (324 female + 146 male) over 598 scan sessions (365 CT + 233 MR). Each of the sessions had an instance of visual function testing available within 6 months of the scan. Visual function was assessed using the American Medical Association Functional Vision Score (FVS), which is calculated based on visual acuity and visual field testing acquired through routine clinical care. FVS is described through a subset of four other scores. The Visual Acuity Scores (VAS) of the left and right eyes was combined with the better VAS of both eyes in a weighted manner to calculate the Functional Acuity Score (FAS). The Visual Field Scores (VFS) of the left and right eyes were combined with the better VFS of both eyes in a weighted manner to calculate the Functional Field Score (FFS). The FVS is calculated using the resulting FAS and FFS. [1]

2.2 Image Processing

Segmentation of the MRI data for computation of image-derived anatomical metrics was based off a previously described multi-atlas segmentation method [2, 3], which automatically segments the optic nerves (including the CSF sheaths), extraocular rectus muscles, eye globes, and orbital fat. This method uses 20 manually labeled atlas images, which include healthy controls as well as ON head drusen, optic neuritis and multiple sclerosis (MS) patients. Four atlases, T1W, T2W, FLAIR and proton density weighted images, each consisting of 20 images, were used in this study. Each target scan type was manually assigned to an atlas. The target image to be segmented was registered to each of the 20 atlas images using an affine registration [4]. The sum of the globe labels was used as a probability map, and the area corresponding to >50% globe probability, or 10 atlases, was used to compute the centroids of the two eye globes. These centroids were dilated by 30mm in the left-right direction, 40mm in the superior-inferior direction, 60mm posterior direction, and 30mm anterior direction. The cropped images were segmented using an affine and non-rigid registration of cropped atlases [5]. The manual labels of the atlas images were transformed to the target space using these registrations and are fused using non-local STAPLE (NLSS) [6, 7].

The multi-atlas segmentation pipeline was used to segment the CT scans, to identify the optic nerves (including the CSF sheaths), extraocular rectus muscles, eye globes, and orbital fat. The segmentation pipeline non-rigidly registered a set of manually labeled example scans to each new patient scan. Next, NLSS was used to combine the labels from each of the examples to identify the orbital structures in the target scan. Kalman filters were used to isolate the Superior Rectus Muscle, Inferior Rectus Muscle, Lateral Rectus Muscle and Medial Rectus Muscle from the muscle labels obtained from the multi-atlas segmentation pipeline [8].

From the segmented orbital structures from the CT and MR pipelines, a MATLAB program computed both traditional radiology measures and novel volumetric metrics and generated a set of descriptive features for each patient. For each of the segmented structures, volume and size features were calculated. These include: volume, maximum diameter, and average diameter for the superior, inferior, medial, and lateral rectus muscles [9–12]; volume and diameter of the globe[13–16]; and length, volume, average area, and maximum diameter of the optic nerve[17,18]. Features that describe the eye orbit as a whole were also calculated.

Author Manuscript Author Manuscript Author Manuscript Author Manuscript

These include: orbital volume; Barrett index[19]; and the volume crowding index[20]. All 21 features are calculated bilaterally for each patient.

2.3 Statistical Modeling

For each of the nine visual function targets (right eye visual acuity score, left eye visual acuity score, both eyes visual acuity score, right eye visual field score, left eye visual field score, both eyes visual field score, functional acuity score, functional field score, functional vision score), a forward stepwise univariate regression procedure (stepwiseglm, MATLAB 2016a, Mathworks, Natick, MA) was conducted with the structural metrics listed above. Significant individual correlates (t statistic) were reported along with the overall model fit (F statistic) and R^2 for each regression. The models were created both with and without incorporating the type of scan (CT/MRI) as a parameter. The models without CT/MRI as a parameter are referred to as "without flags." The models with CT/MRI data as a parameter are referred to as with "flags."

The base regression model (no CT/MRI flags) was $y = \beta_1 x_1 + \cdots + \beta_n x_n$ where y is a visual function metric and $x_1 \cdots x_n$ are structural metrics derived from the CT/MRI data. The regression model with CT/MRI flags was

$$y = \beta_1 x_1 + \cdots + \beta_n x_n + \beta_{CT/MRI} x_{CT/MRI} \quad (1)$$

where $x_{CT/MRI}$ is a 0/1 metric that specifies the type of scan that the structural metrics $x_1 \cdots x_n$ were derived from. The distribution of the response variable was fit to a Poisson distribution.

3. RESULTS

3.1 Image Processing

Using the multi-atlas segmentation pipeline, 1,003 images, consisting of 611 MRI and 392 CT, were labeled with optic nerves (including the CSF sheaths), extraocular rectus muscles, eye globes, and orbital fat. After a manual quality analysis was conducted, 205 MRI images 352 CT images progressed in this research. The eye orbit structural metrics were correctly calculated and aligned with clinical visual function data.

3.2 Statistical Modeling

Each visual function measurement was regressed with all the structural metrics from both eyes as shown in Table 1. These nine regression models were all significant ($p < 0.001$). The structural metrics were separated into left eye structural metrics and right eye structural metrics. RVAS and RVFS were regressed with the right eye structural metrics, and LVAS and LVFS were regressed with the left eye structural metrics. These four regression models were all significant ($p < 0.001$). As noted in Table 1, the fraction of variance (0.067, 0.06, 0.069, 0.067) explained by all four models in the second set of regressions were less than the amounts of variance (0.108, 0.093, 0.113, 0.096) explained in their corresponding models in first set of regressions using structural metrics from both eyes. Each visual function

Author Manuscript Author Manuscript Author Manuscript Author Manuscript

measurement was also regressed with all structural metrics from both eyes and the CT/MRI flag. This third set of regressions shown in Table 1 accounted for whether the structural metrics were acquired from a CT scan or MRI scan. For five out of the nine visual function measurements, incorporating the type of scan into the model allowed the model to explain a greater amount of the variance. Based on this regression result, the structural metrics were separated into CT metrics and MRI metrics to conduct regression functions using only CT scan metrics and only MRI scan metrics. As shown in Table 1, eight out of the nine regressions with only CT scan metrics had higher R-squared values than the corresponding regressions conducted with CT and MRI metrics combined. All nine regressions with only MRI scan metrics had higher R-squared values than the corresponding regressions conducted with CT and MRI metrics combined.

4. CONCLUSION

This research explores the macro relationship between eye orbit structural metrics and visual function measurements. The results indicate a significant relationship between structural and visual metrics. In the models, the reliability of both VAS and VFS increase when stratifying by left and right eye. When including CT/MRI flags, the R-squared values for VAS and VFS in combined CT and MRI derived structural metrics are 0.019 and 0.075, respectively. However, the RVAS/LVAS and RVFS/LVFS R-squared values are 0.108/0.108 and 0.118/0.101. These results held true for the models generated without the flags as well. Observing the right eye and the left eye visual function measurements separately increases the variance that described by the model. Furthermore, analyzing CT and MRI structural metrics separately also increases the amount of variance described across all models. These values are shown in Table 1. Specifically in the case of FFS and FVS, the models including only CT scan structural metrics have R-squared values of 0.128 and 0.133 respectively; the models including only MR scan structural metrics have R-squared values of 0.18 and 0.144; and the combined model values are 0.088 and 0.095.

The analysis in this study was performed on patient data with subjects who suffered from Thyroid Eye Disease, Orbital Inflammation, Optic Nerve Edema, Glaucoma, and Intrinsic Optic Nerve Disease. A large amount of variance in the visual metrics is described by the structural metrics without even separating patients by condition. In the future, the data could be analyzed in specific disease cohorts. This type of analysis could result in more significant correlations between certain structural metrics and visual metrics in relation to given optic condition. Furthermore, the MAS method in conjunction with the structural metric calculation could make it easier to predict what type of care a patient may need in the future. Further study into the association between structural and visual metrics will likely yield interesting insight into the progression of certain diseases and conditions.

Acknowledgments

This project was supported by the National Library of Medicine Grant R25 RFA-HG-14-009, NSF CAREER 1452485 and NIH 5R21EY024036 and was made possible by the Department of Biomedical Informatics at Vanderbilt University, Nashville, TN. The content is solely the responsibility of the authors and does not necessarily represent the official views of the NIH. This work was conducted in part using the resources of the Advanced Computing Center for Research and Education at Vanderbilt University, Nashville, TN. This project was supported

Author Manuscript Author Manuscript Author Manuscript Author Manuscript

in part by ViSE/VICTR VR3029 and the National Center for Research Resources, Grant UL1 RR024975-01, and is now at the National Center for Advancing Translational Sciences, Grant 2 UL1 TR000445-06.

REFERENCES

1. Rondinelli, RD., et al. Guides to the evaluation of permanent impairment. American Medical Association; 2008.
2. Harrigan RL, Panda S, Asman AJ, et al. Robust optic nerve segmentation on clinically acquired computed tomography. Journal of Medical Imaging. 2014; 1(3):034006–034006. [PubMed: 26158064]
3. Panda S, Asman AJ, Khare SP, et al. Evaluation of Multi-Atlas Label Fusion for Orbital Segmentation on In Vivo MRI. Journal of Medical Imaging. 2014
4. Ourselin S, Roche A, Subsol G, et al. Reconstructing a 3D structure from serial histological sections. Image and vision computing. 2001; 19(1):25–31.
5. Avants BB, Tustison NJ, Song G, et al. A reproducible evaluation of ANTs similarity metric performance in brain image registration. Neuroimage. 2011; 54(3):2033–2044. [PubMed: 20851191]
6. Asman AJ, Landman BA. Non-local statistical label fusion for multi-atlas segmentation. Med Image Anal. 2013; 17(2):194–208. [PubMed: 23265798]
7. Asman AJ, Landman BA. Formulating Spatially Varying Performance in the Statistical Fusion Framework. Medical Imaging, IEEE Transactions on. 2012; 31(6):1326–1336.
8. Chaganti, Shikha, Nelson, Katrina, Mundy, Kevin, Luo, Yifu, Harrigan, Robert L., Damon, Steve, Fabbri, Daniel, Mawn, Louise, Landman, Bennett. Structural Functional Associations of the Orbit in Thyroid Eye Disease: Kalman Filters to Track Extraocular Muscles. Proceedings of the SPIE Medical Imaging Conference; February 2016; San Diego, California.
9. Weis E, et al. Clinical and soft-tissue computed tomographic predictors of dysthyroid optic neuropathy: Refinement of the constellation of findings at presentation. Archives of Ophthalmology. 2011; 129(10):1332–1336. [PubMed: 21987676]
10. Hallin ES, Feldon SE. Graves' ophthalmopathy: II. Correlation of clinical signs with measures derived from computed tomography. The British journal of ophthalmology. 1988; 72(9):678–682. [PubMed: 3179255]
11. Ozgen A, Ariyurek M. Normative measurements of orbital structures using CT. AJR. American journal of roentgenology. 1998; 170(4):1093–1096. [PubMed: 9530066]
12. Szucs-Farkas Z, et al. Using morphologic parameters of extraocular muscles for diagnosis and follow-up of Graves' ophthalmopathy: diameters, areas, or volumes? AJR. American journal of roentgenology. 2002; 179(4):1005–1010. [PubMed: 12239055]
13. Weis E, et al. Quantitative Computed Tomographic Predictors of Compressive Optic Neuropathy in Patients with Thyroid Orbitopathy: A Volumetric Analysis. Ophthalmology. 2012; 119(10):2174–2178. [PubMed: 22709420]
14. Szucs-Farkas Z, et al. Using morphologic parameters of extraocular muscles for diagnosis and follow-up of Graves' ophthalmopathy: diameters, areas, or volumes? AJR. American journal of roentgenology. 2002; 179(4):1005–1010. [PubMed: 12239055]
15. Tian S, et al. MRI measurements of normal extraocular muscles and other orbital structures. Graefe's Archive for Clinical and Experimental Ophthalmology. 2000; 238(5):393–404.
16. Pearce E, Bridge H. Is orbital volume associated with eyeball and visual cortex volume in humans? Annals of Human Biology. 2013; 40(6):531–540. [PubMed: 23879766]
17. Rubin PAD, et al. Orbital computed tomographic characteristics of globe subluxation in thyroid orbitopathy. Ophthalmology. 1998; 105(11):2061–2064. [PubMed: 9818606]
18. Peyster RG, et al. High-resolution CT of lesions of the optic nerve. AJR. American journal of roentgenology. 1983; 140(5):869–874. [PubMed: 6601426]
19. Monteiro MLR, et al. Diagnostic ability of barrett's index to detect dysthyroid optic neuropathy using multidetector computed tomography. Clinics. 2008; 63:301–306. [PubMed: 18568237]

Author Manuscript Author Manuscript Author Manuscript Author Manuscript

20. Gonçalves ACP, et al. Quantification of orbital apex crowding for screening of dysthyroid optic neuropathy using multidetector CT. AJNR. American journal of neuroradiology. 2012; 33(8): 1602–1607. [PubMed: 22442048]

21. Lee H, Jilani M, Frohman L, et al. Emergency Radiology. 2004; 10:168. [PubMed: 15290482]

22. Brown HD, Woodall RL, et al. Using magnetic resonance imaging to assess visual deficits: a review. Opthalmic Physiol Opt. 2016

Author Manuscript Author Manuscript Author Manuscript Author Manuscript

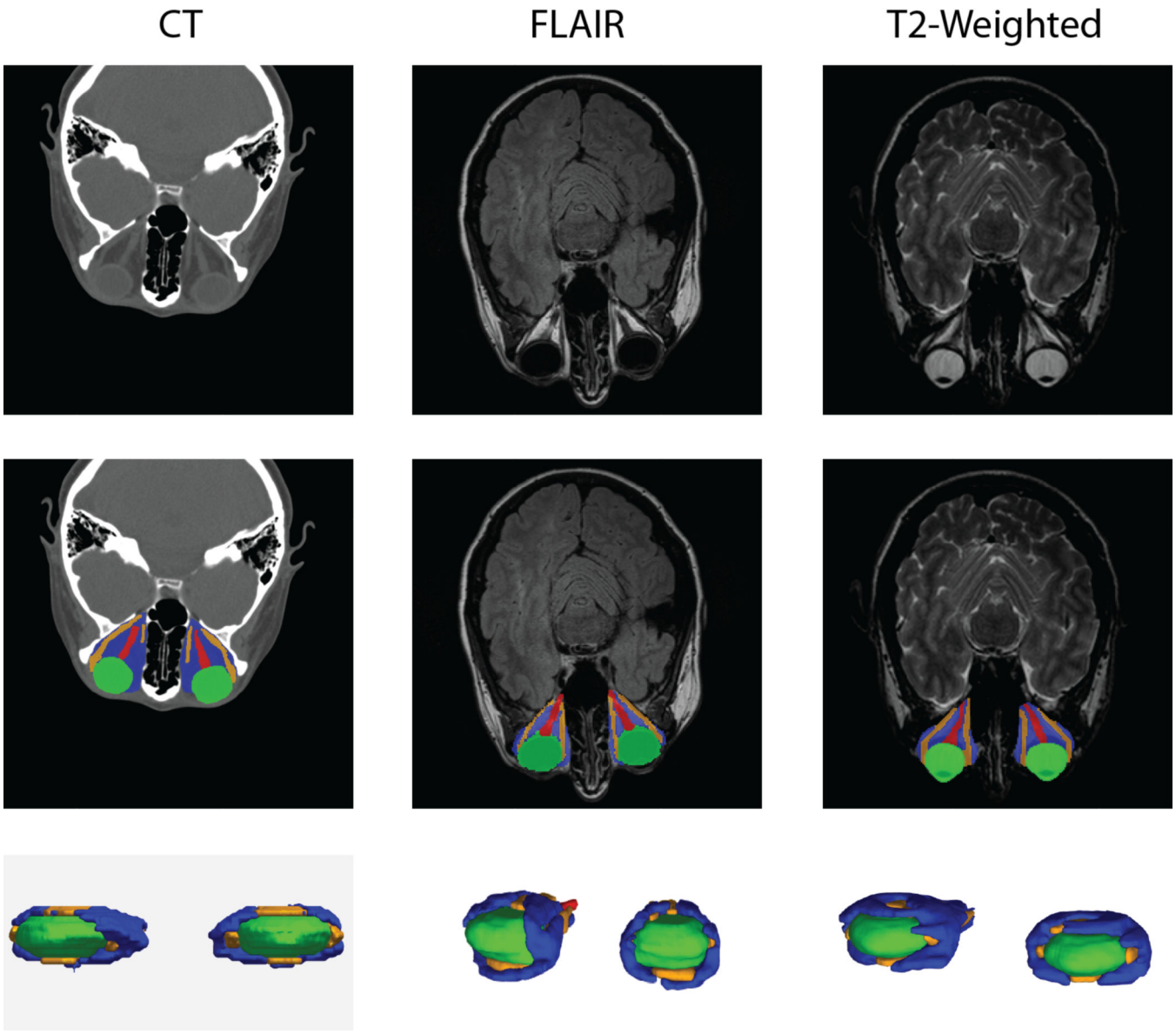

Figure 1.
Example CT and MRI scans (top row) were expertly labeled (center row, lower row) and used in multi-atlas segmentation pipelines.

Author Manuscript Author Manuscript Author Manuscript Author Manuscript

Table 1

ICD9 codes for disease cohorts

Disease	ICD-9 codes	Description
Thyroid Eye Disease	242.00	Toxic diffuse goiter without thyrotoxic crisis or storm
	376.2	Endocrine exophthalmos
	376.21	Thyrotoxic exophthalmos
	376.22	Exophthalmic ophthalmoplegia
Orbital Inflammation	376.0, 376.00	Acute inflammation of orbit
	376.01	Orbital cellulitis
	376.02	Orbital periostitis
	376.1	Chronic inflammation of orbit
	376.11	Orbital granuloma
	376.12	Orbital myositis
	373.13	Abscess of eyelid
Optic Nerve Edema	348.2	Idiopathic intracranial hypertension
	377.0, 377.00	Papilledema
	377.01	Papilledema, increased intracranial pressure
	377.02	Papilledema, decreased ocular pressure
Glaucoma	365.0*	Borderline glaucoma
	365.1*	Open-angle glaucoma
	365.2*	Primary angle-closure glaucoma
	365.3*	Corticosteroid-induced glaucoma
	365.4*	Glaucoma associated with congenital anomalies, dystrophies, and systemic syndromes
	365.5*	Glaucoma associated with disorders of the lens
	365.6*	Glaucoma associated with other ocular disorders
	365.7*	Glaucoma stage, unspecified
	365.8*	Other specified forms of glaucoma
	365.9*	Unspecified glaucoma
Intrinsic Optic Nerve Disease	377.3*	Optic Neuritis
	377.4*	Other disorders of optic nerve

Author Manuscript Author Manuscript Author Manuscript Author Manuscript

Table 2

R-squared Values of Regression Models

R-squared (ordinary)	RVAS	LVAS	VAS	FAS	RVFS	LVFS	VFS	FFS	FVS
All metrics w/o CT/MRI flag	0.108***	0.093**	0.019**	0.041**	0.113**	0.096**	0.075**	0.087**	0.092***
Corresponding eye metrics w/o CT/MRI flag	0.067***	0.06***	-	-	0.069***	0.067***	-	-	-
All metrics w/ CT/MRI flag	0.108***	0.108***	0.019**	0.037***	0.118***	0.101***	0.075***	0.088***	0.094***
All CT scan metrics	0.089***	0.208***	0.142***	0.105***	0.13***	0.127***	0.134***	0.128***	0.133***
All MRI scan metrics	0.27***	0.146***	0.097***	0.11***	0.223***	0.172***	0.179***	0.18***	0.143***

** $p < 0.01$,

*** $p < 0.001$